Microglial activation in the right amygdala-entorhinal-hippocampal complex is associated with preserved spatial learning in *App^NL-G-F* mice

Gloria Biechele [a,1], Karin Wind [a], Tanja Blume [a,b], Christian Sacher [a], Leonie Beyer [a], Florian Eckenweber [a], Nicolai Franzmeier [c], Michael Ewers [b,c], Benedikt Zott [d,e], Simon Lindner [a], Franz-Josef Gildehaus [a], Barbara von Ungern-Sternberg [a], Sabina Tahirovic [b], Michael Willem [f], Peter Bartenstein [a,g], Paul Cumming [h,i], Axel Rominger [a,h], Jochen Herms [b,g,j], Matthias Brendel [a,g,*]

[a] Department of Nuclear Medicine, University Hospital of Munich, LMU Munich, Munich, Germany
[b] DZNE - German Center for Neurodegenerative Diseases, Munich, Germany
[c] Institute for Stroke and Dementia Research, Klinikum der Universität München, Ludwig Maximilian University Munich
[d] Institute of Neuroscience, Technical University of Munich, Munich, Germany
[e] Department of Diagnostic and Interventional Neuroradiology, Klinikum rechts der Isar, Technical University of Munich, Munich, Germany
[f] Chair of Metabolic Biochemistry, Biomedical Center (BMC), Faculty of Medicine, LMU Munich, Munich, Germany
[g] Munich Cluster for Systems Neurology (SyNergy), Munich, Germany
[h] Department of Nuclear Medicine, Inselspital, University Hospital Bern, Bern, Switzerland
[i] School of Psychology and Counselling, Queensland University of Technology, Brisbane, Australia
[j] Center of Neuropathology and Prion Research, University of Munich, Munich Germany

ARTICLE INFO

ABSTRACT

Background: In Alzheimer's disease (AD), regional heterogeneity of β-amyloid burden and microglial activation of individual patients is a well-known phenomenon. Recently, we described a high incidence of inter-individual regional heterogeneity in terms of asymmetry of plaque burden and microglial activation in β-amyloid mouse models of AD as assessed by positron-emission-tomography (PET). We now investigate the regional associations between amyloid plaque burden, microglial activation, and impaired spatial learning performance in transgenic mice *in vivo*.

Methods: In 30 *App^NL-G-F* mice (15 female, 15 male) we acquired cross-sectional 18 kDa translocator protein (TSPO-PET, ^{18}F-GE-180) and β-amyloid-PET (^{18}F-florbetaben) scans at ten months of age. Control data were obtained from age- and sex-matched C57Bl/6 wild-type mice. We assessed spatial learning (i.e. Morris water maze) within two weeks of PET scanning and correlated the principal component of spatial learning performance scores with voxel-wise β-amyloid and TSPO tracer uptake maps in *App^NL-G-F* mice, controlled for age and sex. In order to assess the effects of hemispheric asymmetry, we also analyzed correlations of spatial learning performance with tracer uptake in bilateral regions of interest for frontal cortex, entorhinal/piriform cortex, amygdala, and hippocampus, using a regression model. We tested the correlation between regional asymmetry of PET biomarkers with individual spatial learning performance.

Results: Voxel-wise analyses in *App^NL-G-F* mice revealed that higher TSPO-PET signal in the amygdala, entorhinal and piriform cortices, the hippocampus and the hypothalamus correlated with spatial learning performance. Region-based analysis showed significant correlations between TSPO expression in the right entorhinal/piriform cortex and the right amygdala and spatial learning performance, whereas there were no such correlations in the left hemisphere. Right lateralized TSPO expression in the amygdala predicted better performance in the Morris water maze (β = -0.470, p = 0.013), irrespective of the global microglial activation and amyloid level. Region-based results for amyloid-PET showed no significant associations with spatial learning.

Conclusion: Elevated microglial activation in the right amygdala-entorhinal-hippocampal complex of *App^NL-G-F* mice is associated with better spatial learning. Our findings support a protective role of microglia on cognitive function when they highly express TSPO in specific brain regions involved in spatial memory.

1. Introduction

Alzheimer disease (AD) is the most frequently diagnosed neurodegenerative disease, with burgeoning incidence rates due to the rising life expectancy in industrialized nations (Ziegler-Graham et al., 2008). The neuropathology of AD is histologically characterized by the triad of accumulation of β-amyloid peptide (Aβ) as extracellular plaques, fibrillar tau aggregates within neurons, and the activation of multiple neuroinflammatory pathways, which is marked by activated microglia expressing high levels of the marker 18-kDa translocator protein (TSPO) (Heneka et al., 2015). In humans, regional heterogeneity and asymmetric spatial distribution of neuropathological AD hallmarks is a frequent finding in PET studies (Frings et al., 2015; Ossenkoppele et al., 2016; Tetzloff et al., 2018). This seems of particular importance since as the clinical phenotype of AD depends on the regional localization of tau distribution (Ossenkoppele et al., 2016), whereby verbal memory performance is linked to the usually dominant left hemisphere (Miyashita, 2004). Recently, we showed that regional asymmetric distribution of fibrillar amyloidosis is also evident in several mouse models of amyloidosis (Sacher et al., 2020), in which 14%/ 16% of the mice indicated a strong left/ right hemispheric dominance of the pathology. Moreover, lateralized amyloidosis was positively associated in that study with ipsilateral increases in TSPO expression, which is a surrogate of microglial activation (Sacher et al., 2020). However, whether such a hemispheric asymmetry in amyloid deposition and microglia activity is associated with specific cognitive deficits is unknown.

Performance in the Morris Water Maze (MWM) test is a sensitive indicator of spatial learning in mice (Vorhees and Williams, 2014), and is particularly suited to examine AD-model mice because of its high specificity for hippocampal function (Bryan et al., 2009). Spatial memory, as assessed by MWM, involve the integrated functioning of the hippocampus, the entorhinal cortex and associated structures such as the amygdala and the hypothalamus (Vorhees and Williams, 2014). Importantly, these same brain regions have asymmetry in their anatomical structure and in certain molecular markers (El-Gaby et al., 2015; Goto et al., 2010; Shinohara et al., 2008). This is in line with previous findings that the right hemisphere dominates in spatial learning and memory in rodents (Shinohara et al., 2012; Shipton et al., 2014), as in most humans (Thomason et al., 2009). Yet, there has hitherto been no investigation of possible associations between hemispheric-specific levels of AD-related brain changes and spatial learning performance in rodents.

Given this research gap, our aim was first to explore the regional associations of PET-assessed fibrillar amyloidosis and microglial activation with spatial memory performance in the novel App^{NL-G-F} mouse AD model. Based on our previous results (Ewers et al., 2020), we hypothesized that App^{NL-G-F} mice with low fibrillar amyloidosis and high microglial activation would exhibit better spatial memory. Second, we defined regions of interest for brain regions implicated in spatial memory in order to assess hemispheric differences in the associations between Aβ and TSPO-PET with spatial learning performance. We included the amygdala (Maren, 1999; Sarter and Markowitsch, 1985), the entorhinal cortex (Bannerman et al., 2001) and the hippocampus (Bryan et al., 2009) as target regions of the spatial learning network. Given the reported dominance of the rodent right hemisphere in spatial learning tasks, we hypothesized a lateralization of correlations favoring the right side. Finally, we correlated left and right lateralization of the PET biomarkers with performance in the spatial learning task and validated our PET results by immunohistochemistry and biochemistry. We hypothesized that App^{NL-G-F} mice with an asymmetry of fibrillar amyloid to the left and an asymmetry of microglial activation to the right would express better spatial learning performance.

2. Material and methods

2.1. Experimental design

All experiments were performed in compliance with the National Guidelines for Animal Protection, Germany, with the approval of the regional animal committee (Regierung Oberbayern) and oversight by a veterinarian. All animal experiments complied with the ARRIVE guidelines and were carried out in accordance with the U.K. Animals (Scientific Procedures) Act, 1986 and associated guidelines, EU Directive 2010/63/EU for animal experiments. Animals were housed in a temperature- and humidity-controlled environment with 12-hour light-dark cycle, with free access to food (Sniff, Soest, Germany) and water. Fifteen female and 15 male App^{NL-G-F} mice were imaged by standardized Aβ-PET and TSPO-PET protocols at a mean (SD) age of 10.3 $\pm$ 0.6 months (range: 9.7–12.8 months) (Overhoff et al., 2016). Spatial learning was tested by an established Morris water maze (MWM) protocol (Sacher et al., 2019) within two weeks of PET scanning. To avoid effects of anesthesia, we observed a minimum time gap of five days between the first or last day of spatial learning (including training and probe days) and the closest PET session. The mean (SD) time gap between the probe day and PET examination was 10.6 $\pm$ 2.3 days. Age- and sex-matched C57BL/6 wild-type controls were imaged by Aβ-PET and TSPO-PET (each n=18) and performed the same spatial learning task in MWM (n=14). Biochemistry and immunohistochemistry were performed in a subset of App^{NL-G-F} and wild-type mice.

2.2. Animals

The knock-in mouse model App^{NL-G-F} carries a mutant APP gene encoding the humanized Aβ sequence (G601R, F606Y, and R609H) with three pathogenic mutations, namely Swedish (KM595/596NL), Beyreuther/Iberian (I641F), and Arctic (E618G). Homozygotic App^{NL-G-F} mice progressively exhibit widespread Aβ accumulation first evident at two months of age (Masuda et al., 2016; Saito et al., 2014). Deficits in spatial learning are not observed until six months of age (Whyte et al., 2018) but appear in App^{NL-G-F} mice ranging from 8-12 months of age (Masuda et al., 2016; Sacher et al., 2019). There have been no reports of relevant neuronal loss and atrophy in this model. Age- and sex-matched C57Bl/6 wild-type mice (n=18 for each PET modality) were reanalyzed together with App^{NL-G-F} data and served as control material.

2.3. PET Imaging

2.3.1. PET data acquisition, reconstruction and post-processing

For all PET procedures, radiochemistry, data acquisition, and image pre-processing were conducted according to established, standardized protocols (Overhoff et al., 2016). In brief, ^{18}F-FBB Aβ-PET recordings (average dose: 11.7$\pm$2.1 MBq) with an emission window of 30–60 min after injection were obtained to measure fibrillar cerebral amyloidosis. ^{18}F-GE-180 TSPO-PET recordings (average dose: 11.4$\pm$1.9 MBq) with an emission window of 60–90 min after injection were performed for assessment of cerebral TSPO expression. Isoflurane anesthesia was induced before tracer injection and maintained to the end of the imaging time window.

2.3.2. PET image analysis

All analyses were performed using PMOD (version 3.5; PMOD technologies, Basel, Switzerland). Static 30–60 min and 60–90 min image frames were co-registered to tracer specific templates (mixed App^{NL-G-F} and wild-type templates) by a manual rigid-body transformation (TX$_{rigid}$) (Overhoff et al., 2016). In the second step, we performed a reader-independent fine co-registration to the tracer specific

templates (Overhoff et al., 2016). Here, the initial manual fused images were normalized by non-linear brain normalization (TX$_{BN}$) via the PMOD brain normalization tool (equal modality; smoothing by 0.6 mm; nonlinear warping; 16 iterations; frequency cutoff 3; regularization 1.0; no thresholding). We then applied the concatenation of TX$_{rigid}$ and TX$_{BN}$ to obtain optimal spatial resampling with a minimum of interpolation. Normalization of emission images to standardized uptake value ratio (SUVR) images was performed using the previously validated mesencephalic periaqueductal gray (PAG, 20 mm^3) (Sacher et al., 2019). Four ROIs were defined bilaterally in the amygdala (3 mm^3 each), the entorhinal/piriform cortex (5 mm^3 each), the hippocampus (2 mm^3 each) and the frontal cortex (12 mm^3 each, **Supplemental Figure 1**). Target to PAG SUVR values of Aβ-PET and TSPO-PET were obtained for each bilateral region. The TSPO/Aβ ratio was calculated by division of the SUVR values of both tracers in a single region to generate a quantitative index of microglial response relative to a given amount of fibrillary amyloidosis. For each bilateral region, the hemispheric asymmetry index (AI) was calculated for TSPO-PET, Aβ-PET SUVR, and the TSPO/Aβ ratio using the formula:

$$AI[\%] = 200 \times (L - R)/(L + R)$$

2.4. Behavioral testing

All 30 *App^{NL-G-F}* mice and 14 age- and sex-matched C57BL/6 wild-type mice underwent a MWM test of spatial learning and memory deficits, which was performed according to a standard protocol with small adjustments (Bromley-Brits et al., 2011) as previously described (Sacher et al., 2019). In brief, the first test day served for acclimatization with the platform visible (5 min per mouse). Then the mice underwent five training days where each mouse had to perform four trials per day with the platform visible on the first training day and the platform hidden under water for all other training days. The test day entailed a single trial with complete removal of the platform. The maximum trial length on all training and test days was set to a maximum of 70 s. The video tracking software EthoVision® XT (Noldus) was used for analyses of escape latency, the platform frequency, and attendance in the platform quadrant at the probe trial. Eight wild-type mice were assessed together with the *App^{NL-G-F}* model, whereas six wild-type mice were examined two months apart and included to increase to statistical power of the control cohort. Aiming to increase the robustness of MWM results, we conducted a principal component analysis (PCA) of all single MWM readouts as indicated in the statistics section. Thus, we obtained a single quantitative index of MWM performance per mouse for correlation with PET imaging results.

2.5. Immunohistochemical and biochemical validation

Biochemical analyses were performed in samples from the entire forebrain in seven *App^{NL-G-F}* mice (4 female, 3 male) and four wild-type mice (2 female, 2 male). Soluble Trem2 protein was extracted from brain tissue with Tris-buffered saline, and measured by ELISA, using polyclonal sheep antibody for coating (AF1729; R&D Systems) and biotinylated polyclonal sheep antibody (BAF1729; R&D Systems) together with streptavidin-horseradish peroxidase (N-100; ThermoFisher Scientific) for detection.

Brains intended for immunohistochemistry were fixed by immersion in 4% paraformaldehyde at 4 °C for 14 h. Nine *App^{NL-G-F}* mice (5 female, 4 male) and four wild-type mice (2 female, 2 male) were analyzed. Two representative 50 μm-thick slices per animal were then cut in the axial plane using a vibratome (VT 1000 S, Leica, Wetzlar, Germany). Free-floating sections were permeabilized with 2% Triton X-100 overnight and blocked with I-Block™ Protein-Based Blocking Reagent (Thermo Fischer Scientific). We obtained immunohistochemical labelling of microglia using an Iba-1 primary antibody (dilution; Wako, 1:200), and the A-21244 secondary antibody (Invitrogen, 1:500). The unbound dye

was removed by three washing steps with PBS, and the slices were then mounted on microscope slides with fluorescent mounting medium (Dako, Germany). Images were acquired on inverted confocal Laser-Scanning Microscope LSM780 (Zeiss). We imaged four different positions in the CA1-Region of the hippocampus of each slice 3-dimensional with a Plan-Apochromat 40x/1.4 Oil DIC M27 (Zeiss) objective The 3-dimensional image stacks (2048 × 2048 × 123 pixels (lateral pixel size: 0.17 μm, axial pixel size: 0.40 μm), zoom 0.6, pixel dwell 0.79 μs) were maximum-intensity-projected. The Iba-1 load (area-%) was calculated as the summed area of all Iba-1 positive cells relative to the area of regions of interest using an automated threshold in ImageJ software.

2.6. Statistical Analysis

2.6.1. Sample size estimation

An orienting sample size estimation (G*Power, V3.1.9.2, Kiel, Germany) was based on our previous data on PET imaging and spatial learning in *App^{NL-G-F}* and wild-type mice (Sacher et al., 2019). A t-test estimation with two independent means using α = 0.05 and a power of 0.8 for Aβ-PET in the hippocampus computed a minimal necessary sample size of n = 12 per group to detect the observed 3.2 % difference in signal (standard deviation per group: 0.025 SUVr) at 10 months of age between *App^{NL-G-F}* and wild-type mice. A regression estimation (fixed model) using α = 0.05 and a power of 0.8 for a partial R^2 of 0.2 (based on previous PET/MWM correlations) computed a necessary sample size of n = 27.

2.6.2. Statistical parametric mapping (SPM) group comparisons

For both tracers, whole-brain voxel-wise comparisons of PAG-scaled SUVR images between groups of *App^{NL-G-F}* and wild-type mice were performed by an unpaired Student's *t*-test as described previously (Rominger et al., 2013).

2.6.3. SPM regression analyses

In preparation for the correlation analyses between spatial learning scores and PET readouts, we extracted the principal component of the MWM test from three spatial learning readouts (escape latency, frequency of attaining platform, time spent in platform quadrant) using SPSS 25 statistics (IBM Deutschland GmbH, Ehningen, Germany). Prior to the PCA, we tested the linear relationship of the data by a correlation matrix, and discarded any items with a correlation coefficient < 0.3. We used the Kaiser-Meyer-Olkin (KMO) measure and Bartlett's test of sphericity to test for sampling adequacy and suitability for data reduction. Components with an Eigenvalue > 1.0 were extracted and a varimax rotation was selected. Subsequently, a voxel-wise regression analysis was performed in *App^{NL-G-F}* mice using PAG-scaled SUVR images as the dependent variable and the principal component of spatial learning as independent variable. Age and sex served as covariates for the regression analysis. All SPM analyses were corrected for multiple comparisons by a false discovery rate (FDR) correction (Benjamini and Hochberg, 1995). To avoid bias by regional constitution of single voxels (Chumbley and Friston, 2009), we used a 3-dimensional grid of squared regions of interest (0.8 × 0.8 × 0.8 mm each) across the brain to obtain a topological FDR correction (Chumbley and Friston, 2009). An FDR-corrected *p*-value of 0.05 was set as the threshold for voxel-wise analyses.

2.6.4. Region based regression analyses

SPSS was used for region-based analyses. Regression coefficients (β) were computed between target region SUVR values of TSPO-PET or Aβ-PET images or the TSPO/Aβ ratio with the principal component of spatial learning performance using a multivariate model in *App^{NL-G-F}* mice, controlled for age and sex. The association between the regional asymmetry index of the TSPO/Aβ ratio and the principal component of spatial learning in *App^{NL-G-F}* mice was computed by a multiple regression model together with age, sex and the absolute biomarker value per region (mean of both hemispheres). We applied an FDR-correction to account for multiple testing with predefined regions of interest. Next, we
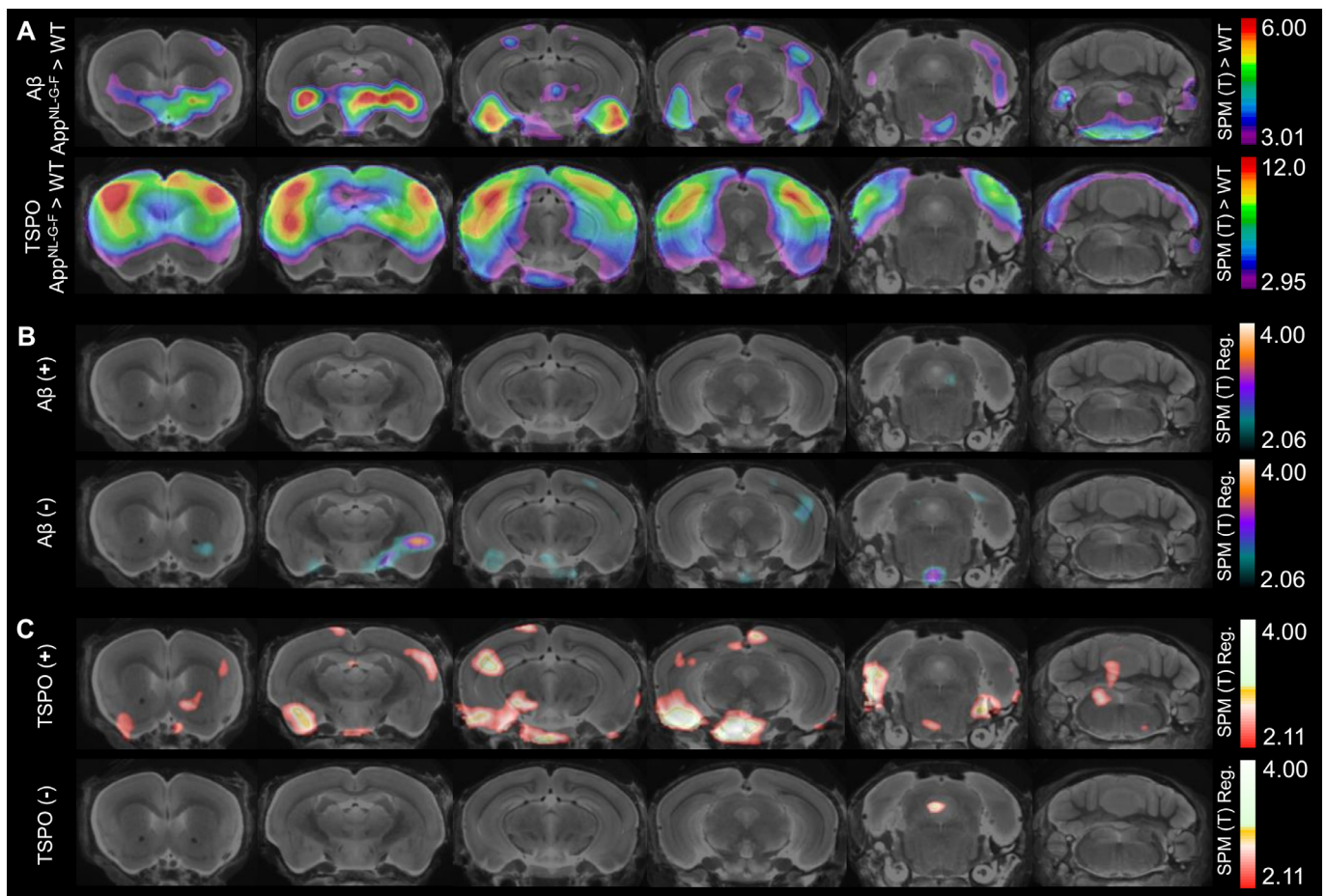
Fig. 1. *Voxel-based analyses by statistical parametric mapping (SPM):* Coronal images display group-wise PET analyses projected upon a MRI standard template at different slices. (**A**) Color coding shows the statistical significance of the contrast between Aβ- and TSPO-PET signals App^{NL-G-F} mice (n=30) versus wild-type controls (n=18). Highest levels of fibrillar amyloidosis were observed by Aβ-PET in entorhinal and piriform cortices, as well as in the thalamus and the striatum, whereas TSPO-expression respresening activated microglia was predominantly elevated in frontal and parietal cortices and in the hippocampus. (**B**) Few clusters in which Aβ-PET uptake correlated negatively with spatial learning performance when assessed by voxel-wise regression analysis in App^{NL-G-F} mice (n=30) and no clusters of positive correlation between Aβ-PET uptake and spatial learning performance. (**C**) Positive correlation clusters between spatial learning performance with higher microglial activation were observed in the App^{NL-G-F} mice (n=30) predominantly in the amygdala, the entorhinal and piriform cortices, the hippocampus, and the hypothalamus. All SPM T-scores represent a false discovery rate corrected p-value threshold of < 0.05. All analyses were controlled for age and sex. SPM – statistical parametric mapping, MRI – magnet resonance imaging, Aβ – beta amyloid, TSPO – 18 kDa translocator protein, EL – escape latency, FQ – frequency of platform crossings, QU – time spent in the platform quadrant, (+) – positive association, (-) – negative association, Reg. – regression analysis, R – right, L = left.

computed the association between sTrem2 or Iba-1 area-% and the principal component of spatial learning in App^{NL-G-F} mice by a regression model together with age and sex. Single MWM readouts, sTrem2 and Iba-1 area-% values were compared between App^{NL-G-F} and wild-type mice by an unpaired Student's t-test. A p-value of less than 0.05 was considered to be significant for rejection of the null hypothesis.

2.7. Data/code availability statement

Imaging data are available in nifti format and can be transferred upon request by the corresponding author. Behavioral, biochemical and immunohistochemical data are available in table format on Mendeley Data.

3. Results

3.1. Microglial activation shows stronger associations with impaired spatial learning in App^{NL-G-F} mice than did fibrillar amyloidosis

Voxel-based analyses of Aβ-PET and TSPO-PET SUVR in App^{NL-G-F} mice versus wild-type controls showed the expected widespread fibrillar

amyloidosis and microglial activation throughout the brain of the transgenic mice (Fig. 1A). We found the highest levels of fibrillar amyloidosis in entorhinal and piriform cortices and the thalamus, whereas microglial activation was predominantly elevated in frontal and parietal cortices as well as in the hippocampus (Fig. 1A). Behavioral test results showed that App^{NL-G-F} mice had prolonged escape latency (19.9 ± 12.8 s vs. 13.0 ± 6.7 s, $p = 0.023$) but only minor differences in platform crossings (3.2 ± 1.8 vs 4.0 ± 2.1, $p = 0.219$) or time spent in the platform quadrant (17.5 ± 6.2 s vs. 18.3 ± 3.4 s, $p = 0.630$) when compared to wild-type mice. Given the vulnerability of single MWM readouts to variability, we conducted a PCA to generate a more robust MWM performance index per mouse. The PCA resulted in a KMO sampling adequacy of 0.610 and a significant Bartlett's test of sphericity ($p = 0.001$). We found one principal component with an Eigenvalue of 1.730, which explained 58% of the variance. The component matrix was 0.825 for platform crossings, -0.780 for escape latency and 0.664 for time spent in the platform quadrant.

There were only few spatially dispersed voxel clusters where fibrillar amyloidosis correlated negatively with spatial learning performance in App^{NL-G-F} mice and no significant clusters of positive association between fibrillar amyloidosis and spatial learning performance (Fig. 1B). Voxel-wise TSPO-PET SUVr in the transgenic mice had strong positive

Table 1
Regression coefficients between microglia PET and spatial learning.

TSPO	Amygdala	Entorhinal/Piriform cortex	Hippocampus	Frontal cortex
Right	0.481*	0.578*	0.402	0.322
P	0.038	0.010	0.091	0.126
Left	0.182	0.339	0.382	0.285
P	0.353	0.124	0.089	0.162
TSPO/Aβ Ratio	Amygdala	Entorhinal/Piriform cortex	Hippocampus	Frontal cortex
Right	0.602**	0.542*	0.375	0.338
P	0.006	0.012	0.098	0.105
Left	0.300	0.358	0.400	0.336
P	0.121	0.099	0.093	0.091
β-amyloid	Amygdala	Entorhinal/Piriform cortex	Hippocampus	Frontal cortex
Right	-0.343	-0.258	-0.010	0.011
P	0.589	0.492	0.958	1.000
Left	-0.256	-0.189	-0.208	-0.179
P	0.695	0.538	0.578	0.484

Regression coefficients (β) are given for TSPO-PET quantification, the TSPO/Aβ-ratio and fibrillar Aβ in predefined brain regions with the principal component of Morris water maze, controlled for age and sex. False discovery rate correction was performed for eight regions of interest.

 * $p < 0.05$.
 ** $p < 0.01$.

correlations with spatial learning performance predominantly in the amygdala, entorhinal and piriform cortices, the hippocampus, and the hypothalamus (Fig. 1C). There were no relevant clusters indicating an association between high TSPO-PET SUVr and worse spatial learning (Fig. 1C).

3.2. Microglial activation is associated with better spatial learning predominantly in the right amygdala-entorhinal-hippocampal complex

For making detailed comparisons of hemispheric differences in spatial learning associations, we defined homologue regions of interest in brain areas known for their involvement in spatial learning tasks (amygdala, entorhinal/piriform cortex, hippocampus (Vorhees and Williams, 2014)), and in the frontal cortex. An elevated TSPO-PET signal in these predefined regions of App^{NL-G-F} mice was associated with better spatial learning when controlled for age and sex (Table 1) in the right amygdala ($\beta = 0.481$, $p = 0.038$) and the right entorhinal/piriform cortex ($\beta = 0.578$, $p = 0.010$). We observed no significant associations between TSPO-PET in the hippocampus and the frontal cortex with spatial learning. We next tested to see if the observed TSPO-PET associations were influenced by the individual regional burden of fibrillar amyloidosis, finding that the corresponding associations for the TSPO/Aβ ratio were similar to those for the stand-alone TSPO-PET readout (Table 1).

Correlation plots for the Aβ-corrected TSPO-PET (TSPO/Aβ ratio) with MWM escape latency are illustrated in Fig. 2A. The observed associations were also discernible in individual mice with especially high or low TSPO-PET SUVr in the right amygdala-entorhinal-hippocampal complex (compare Figs. 2B & 2C). There were no significant associations of region-based fibrillar amyloidosis with spatial learning performance (Table 1).

3.3. Asymmetric microglial activation in the amygdala is associated with spatial learning

Next, we asked if the lateralization of microglial activation in individual App^{NL-G-F} mice has an independent impact on the spatial learning performance. To answer this, we computed a regression model with regional asymmetry (assessed by the AI) and spatial learning performance,

controlled for the absolute individual amount of TSPO-PET quantification (mean TSPO/Aβ ratio of both hemispheres), age and sex.

Regional lateralization of the TSPO/Aβ ratio was predominantly on the right side for the frontal cortex (19 vs. 11) and predominantly on the left side for the amygdala (22 vs. 8), entorhinal/piriform cortex (22 vs. 8) and hippocampus (18 vs. 12). Strong asymmetries ($|AI| > 4.5\%$) were observed at a similar frequency (left 32%, right 15%) when compared to our previous findings in the same mouse model (Sacher et al., 2020). Right lateralized AI of the TSPO/Aβ ratio in the amygdala predicted better spatial learning performance in App^{NL-G-F} mice ($\beta = -0.470$, $p = 0.013$), independent of the mean bilateral TSPO/Aβ ratio, age and sex (Fig. 3A). The regression model of microglial activation in the amygdala and their asymmetry together with sex and age explained 41% of the variance in spatial learning performance ($F_{(4,25)} = 6.03$, $p = 0.006$, $R^2 = 0.49$, $R^2_{adjusted} = 0.41$). Explanation of spatial learning performance by models including the entorhinal/piriform cortex and the hippocampus did not reach significance ($F_{(4,25)} = 3.34$, $p = 0.051$, $R^2 = 0.35$, $R^2_{adjusted} = 0.24$ / $F_{(4,25)} = 2.25$, $p = 0.124$, $R^2 = 0.26$, $R^2_{adjusted} = 0.15$), both without a significant impact by asymmetry on the model (Fig. 3B,C). The cortical model did not significantly explain variance in spatial learning performance ($F_{(4,25)} = 1.47$, $p = 0.240$, $R^2 = 0.19$, $R^2_{adjusted} = 0.06$, Fig. 3D).

3.4. Immunohistochemistry and sTrem2 support a protective role of activated microglia on spatial learning

To validate our *in vivo* PET findings, we performed Iba-1 immunohistochemistry and measures of sTrem2 in brain sections and whole brain lysate. sTrem2 concentration was 4.2-fold higher in App^{NL-G-F} mice when compared to wild-type mice (39.7 vs. 9.5 ng/ml, $p < 0.001$, Fig. 4A). sTrem2 and the principal component of spatial learning showed a positive association in App^{NL-G-F} mice after controlling for age and sex ($\beta = 0.707$, $p = 0.038$, Fig. 4B). The Iba-1 area-% was 4.4-fold higher in App^{NL-G-F} when compared to wild-type mice (10.6 vs. 2.4 %, $p < 0.001$, Fig. 4C). The Iba-1 area-% and the principal component of spatial learning showed a positive association in App^{NL-G-F} mice after controlling for age and sex ($\beta = 0.705$, $p = 0.047$, Fig. 4D, E). In summary, we find congruent data between *in vivo* TSPO-PET and *ex vivo* methods.

4. Discussion

We present the first preclinical *in vivo* investigation aiming to elucidate regional associations of fibrillar plaque burden and TSPO expression with performance of a spatial learning task in an Aβ mouse model. In App^{NL-G-F} mice, we observed significant correlations of better MWM performance with high TSPO expression in brain regions matching the known networks of spatial memory processing. In contrast, there were distinctly weaker associations of spatial learning scores with fibrillar Aβ burden. Furthermore, the associations between higher TSPO expression and better spatial learning were stronger in right hemispheric brain regions of App^{NL-G-F} mice, and of much lower significance in the left hemisphere. The presence of lateralized TSPO expression in the amygdala predicted spatial learning performance independent of absolute TSPO expression and amyloidosis, and with adjustment for age and sex of the individual App^{NL-G-F} mice.

We found an association between better spatial learning and high TSPO expression in the novel AD mouse model App^{NL-G-F}. We have shown earlier that TSPO expression measured with ^{18}F-GE-180 PET provides a good surrogate of microglial activation in AD model mice as demonstrated by immunohistochemistry (Overhoff et al., 2016; Parhizkar et al., 2019; Sacher et al., 2019). These cognitive/behavioral correlates of increased TSPO binding are in line with our preliminary data in a small cohort of PS2APP mice (Focke et al., 2019). There, we did not find direct associations of TSPO expression and spatial learning at a single time point, but higher early TSPO expression at 8 months predicted preserved spatial learning at 13.5 months. Our novel data in
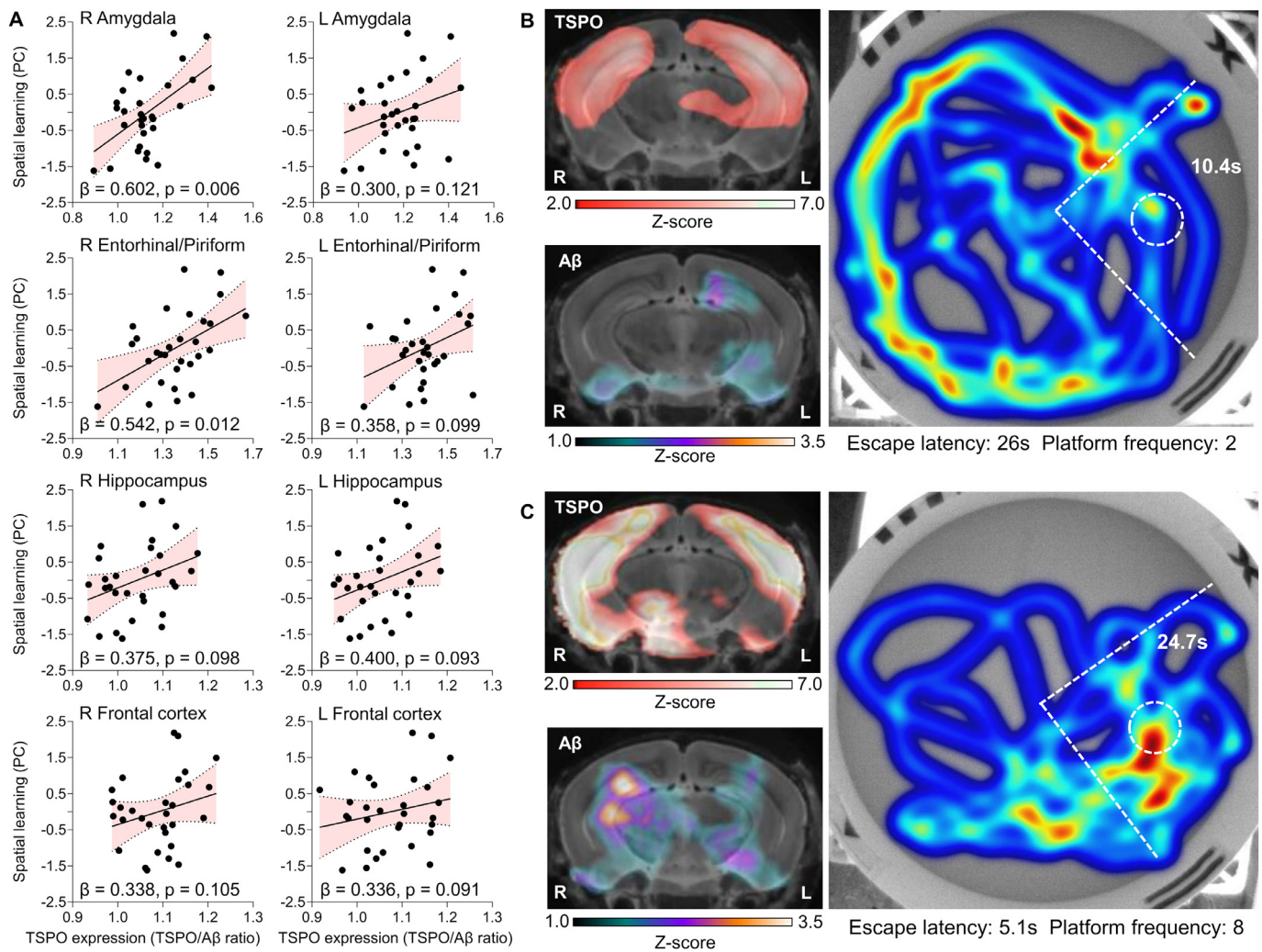
Fig. 2. *Region-based regression analyses of microglial activation and spatial learning: (A)* The principal component of Morris water maze readouts is illustrated as a function of standardized-uptake-value ratios for TSPO-PET quantification (corrected for Aβ-PET quantification) separately for right and left hemispheric regions. Microglial activation of *App^{NL-G-F}* mice ($n = 30$) was significantly associated with spatial learning performance in the right amygdala and in the right entorhinal and piriform cortices. Regression analysis was performed with adjustment for age and sex and with false discovery rate correction for eight regions of interest. The error band represents the 95% confidence interval (**B, C**) Water maze heat map comparison (residency on the test day) of representative individual *App^{NL-G-F}* mice with low (**B: top**) and high (**C: bottom**) Microglial activation in the right amygdala-entorhinal-hippocampal complex. Distribution of fibrillar amyloidosis was similar in both mice. Dashed lines show the platform quadrant and dashed circles show the platform location during training days. TSPO – 18 kDa translocator protein, PET – positron-emission-tomography, Aβ – beta amyloid, s – seconds; R = right; L = left.

a large group of ($N = 30$) *App^{NL-G-F}* mice aged 11 months implies that present or ongoing microglial activation in response to primary amyloidosis can be beneficial for brain function. *Prima facia*, one might have expected that elevated expression of microglia, which are the resident brain macrophages, would suggest a more fulminant and damaging inflammatory process. Thus, the present findings might be consistent with the polarized functionality of microglia, which have pro- and anti-inflammatory phenotypes (Chen et al., 2018), supporting a protective role of microglia on cognitive function when they express TSPO. Importantly, the present findings of an association between better spatial learning performance in AD-model mice and microglial activation were predominantly observed in the amygdala-entorhinal-hippocampal complex and related regions, which are directly involved in spatial learning. Since the corresponding structures together comprise a proportion of the rodent brain, it is not surprising that we were able to reproduce our PET observations by sTrem2 measures in whole brain lysate. However, the regions involved in spatial learning in the human brain are small in relation to whole brain volume, such that a similar association in AD patients might not manifest in measurable effects on the microglial

markers such as soluble Trem2 in cerebrospinal fluid (Suarez-Calvet et al., 2016). This highlights the advantage of region-specific microglia measures afforded by molecular imaging with PET. Iba-1 immunohistochemistry for activated microglia, which also showed a positive association between spatial learning performance with hippocampal microglial activation also validate our *in vivo* TSPO-PET results.

The increased TSPO expression in the right amygdala and the entorhinal/piriform cortex of *App^{NL-G-F}* mice was of small magnitude relative to basal expression in wild-type mice, whereas the corresponding increases in frontal cortex and hippocampus were more pronounced. Nonetheless, increased fibrillar Aβ binding was of equal or higher magnitude in the frontal cortex and the hippocampus (see Figure 1A & Supplemental Figure 2). Longitudinal PET data in *App^{NL-G-F}* mice indicated slower accumulation of fibrillar Aβ in mice with high TSPO expression at baseline (Ewers et al., 2020), which could indicate that a trait of high activation of microglia in the amygdala-entorhinal-hippocampal complex bodes well for an individual's capacity to cope with Aβ accumulation. This fits with the observation of a cluster-based association
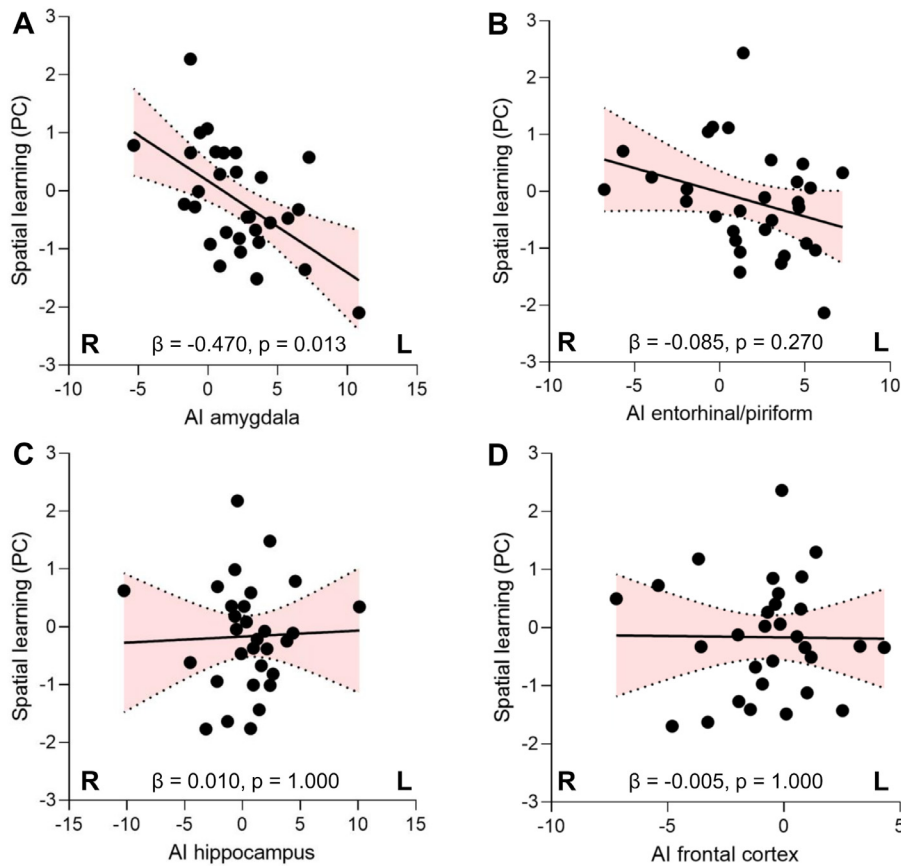
Fig. 3. *Regression analysis of asymmetry:* Partial regression plots illustrate the association between the asymmetry index (AI) of TSPO-PET in different predefined brain regions and spatial learning (principal component, PC) of App^{NL-G-F} mice (n=30). Regression analysis was performed with controlling for age, sex and the bilateral value of TSPO-PET. The TSPO/Aβ ratio was used to control for fibrillary regional Aβ levels. False discovery rate correction was performed for the four regions of interest. The error band represents the 95% confidence interval. R = right, L = left.

between lower fibrillar Aβ and longer time spent in the platform quadrant (Fig. 1). The present cross-sectional design does not support causal inference, but the results may support the hypothesis that increased TSPO expression is a marker for enhanced microglial removal of Aβ in App^{NL-G-F}, with consequences for preserved brain function. However, we note there were only minor associations of the Aβ-PET signal with other spatial learning readouts. This gives further evidence that the fibrillar Aβ burden detectable by PET may have only limited impact on present cognition, which is also supported by human clinical data (Jagust et al., 2009). We note that soluble or non-fibrillar Aβ may yet impair spatial learning in Aβ mouse models (Huber et al., 2018).

The second goal of our study was to elucidate the functional impact of the asymmetric distribution of PET biomarkers, which we have amply documented in Aβ PET studies of various AD mouse models (Sacher et al., 2020). In this regard, we find clear predominance of right hemispheric associations between TSPO expression and spatial learning readouts. This fits with earlier reports that the right hemisphere is especially involved in spatial learning tasks for rodents (Shinohara et al., 2012; Shipton et al., 2014), as is likewise the case in humans (Thomason et al., 2009). The weaker effects observed for left hemispheric regions underpin the hypothesis that the protective effect of microglial activation on spatial learning performance is seemingly specific for the right hemisphere. In this regard, it would be of interest to evaluate if our present findings also hold for brain functions localized in the left hemisphere, such as verbal semantic memory in most humans (Zahn et al., 2004) or auditory brain function in mice (Ehret, 1987). Interestingly, the present pattern of association between TSPO-PET and spatial learning in App^{NL-G-F} matches the preliminary findings in our pilot investigation of PS2APP mice (Focke et al., 2019). While that previous study in a small sample of (n=10) PS2APP mice did not allow us to draw robust conclusions, the current data further strengthen the view that spatial learning performance is preserved when microglia are activated in the amygdala-

entorhinal-hippocampal complex of the right hemisphere. Indeed, we saw the strongest behavioral impact of asymmetric TSPO expression in the amygdala. Here, we even found an association of the MWM endpoint with the lateralization of TSPO expression, independent from the absolute amygdaloidal TSPO expression, with correction for effects of amyloidosis, age and sex. Previous structural imaging studies indicate that amygdala volumetric asymmetry increasing in normal human aging (Pedraza et al., 2004), which bears some relation with subjective cognitive decline (Yue et al., 2018). Furthermore, the amygdala has important regulatory functions in memory tasks (Roozendaal et al., 2004), which seemingly fits with the strong associations in App^{NL-G-F} mice between spatial learning performance with asymmetric TSPO expression in amygdala. Notably, we did not see any relationship between asymmetric TSPO expression and asymmetric fibrillar amyloidosis in the amygdala and the entorhinal/piriform cortex of App^{NL-G-F} mice, whereas there was a clearly positive correlation in frontal cortex and hippocampus (Supplemental Figure 2). This could potentially indicate a lesser coupling between amyloidosis and microglial activity in the inferior parts of the amygdala-entorhinal-hippocampal complex when compared to that in the cortex (Sacher et al., 2020). This implies that unknown factors may mediate regional differences in the coupling between Aβ overexpression and the microglial response. This phenomenon might be investigated using cell culture techniques or high-resolution immunohistochemical examination of the spatial association between polarized microglia and amyloid plaques.

One strength of our study lies in multimodal molecular imaging of AD biomarkers in conjunction with a behavioral test of spatial learning in a large cohort of App^{NL-G-F} mice. Future studies of this type could include a longitudinal component to support causal inferences about the impact of baseline microglial expression on responses to amyloid overexpression or determine the biochemical thresholds sufficient for effects on cognition. In addition, one might test the effect of microglial activa-
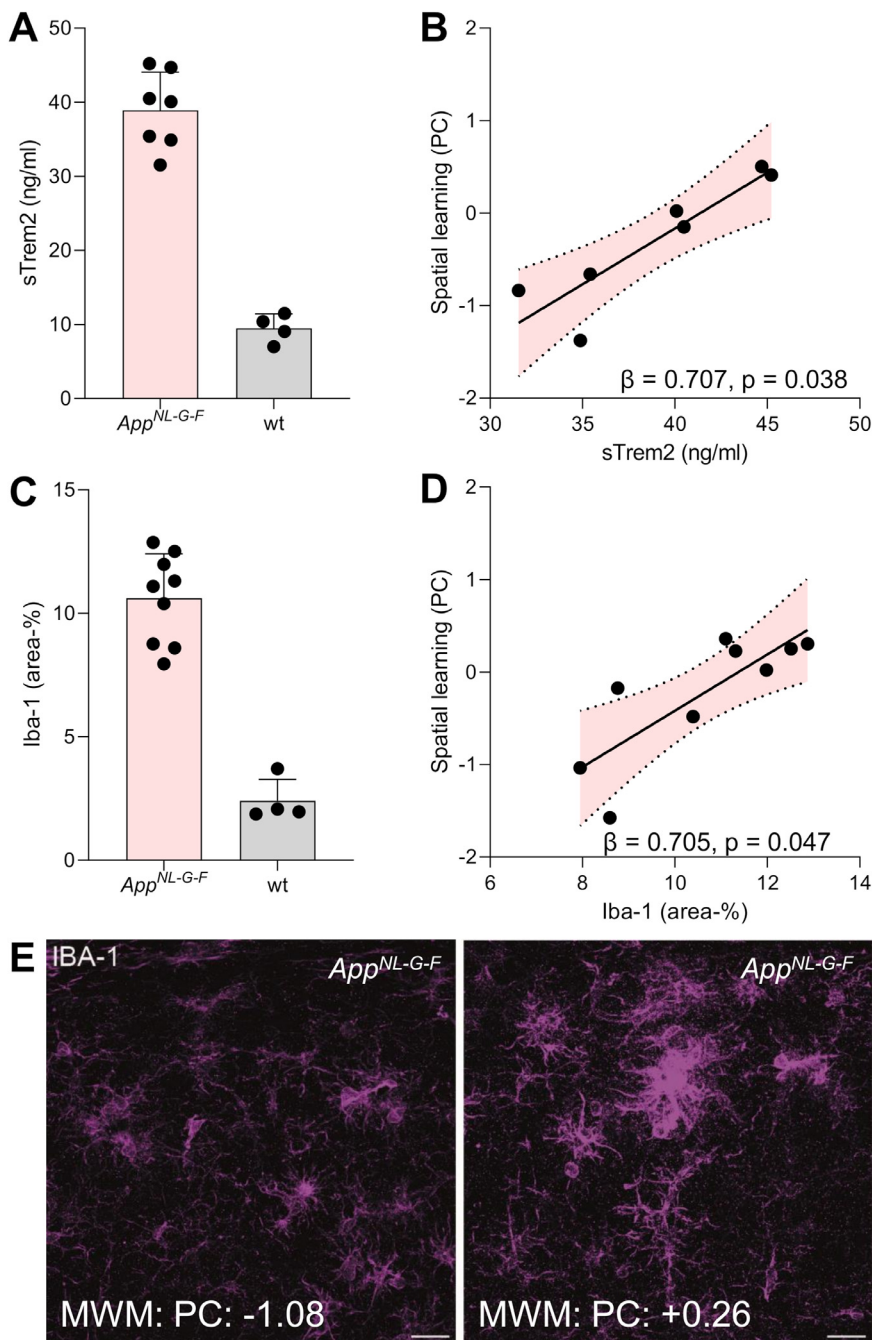
Fig. 4. *Biochemical and Immunohistochemical validation:* Elevated levels of sTrem2 in *App*[NL-G-F] mice (n=7, **A**) were positively associated with spatial learning performance (**B**). Similarly, increased Iba-1 immunoreactivity in the hippocampus of *App*[NL-G-F] mice (*n*=9, **C**) was positively associated with spatial learning performance (**D**). Regression analysis was performed with controlling for age and sex. The error band represents the 95% confidence interval. (**E**) Individual *App*[NL-G-F] examples with low (left) and high (right) Iba-1 immunoreactivity in the hippocampus show deteriorated (left) and preserved (right) spatial learning performance. Scale bar = 20 μm. PC = principal component of Morris water maze (MWM); wt = wild-type.

tion with lipopolysaccharide treatment on the progression of amyloidosis and cognitive changes in AD model mice. Ultimately, present results force us to consider that individual mice of the same genetic background are not clones or carbon copies, but that unknown factors determine their individual trajectories with respect to asymmetric expression of biomarkers and cognition. We did not include volumetric analyses in our study design since earlier reports did not reveal relevant brain atrophy in aging *App*[NL-G-F] mice (Masuda et al., 2016; Saito et al., 2014). However, we note that hybrid imaging systems such as small animal PET/MRI (Frost et al., 2020) could be of interest to study interaction effects between microglial activation, spatial learning deficits, and atrophy in models with neuronal loss, such as tau models. Among the limitations of our study, we note that spatial learning tasks as MWM have a high methodological variance (Vorhees and Williams, 2006). I.e. hitting the place of the platform during first crossing of the basin

by chance can lead to false low escape latency, whereas resting at the wall in the platform quadrant can cause spuriously long times spent in the platform quadrant. Therefore, we used a principal component analysis of common MWM readouts to improve the robustness of the data in single animals, as has been used previously in spatial learning evaluations of amyloid mouse models (Vorhees and Williams, 2006, 2014; Whyte et al., 2018). Present results will support power calculation for the design of subsequent intervention studies entailing a correlation analyses between MWM and PET endpoints, and we note that results in individual mice require cautious interpretation. We also note that Aβ plaques in *App*[NL-G-F] mice have only low proportions of fibrillar Aβ, which present the primary binding pocket of this and other fluorinated Aβ PET tracers (Catafau et al., 2016). Thus, Aβ PET may not depict the most toxic component of the increased amyloid expression in *App*[NL-G-F] mice. Also, we used the hippocampus as a representative target

region for immunohistochemistry validation of microglial activation in the amygdala-entorhinal-hippocampal complex, and note as a limitation of the present study that we did not separately access Iba-1 staining in the amygdala and the entorhinal cortex. The association between spatial learning score and microglial activation in the predefined hippocampus region did not survive correction for multiple comparisons, but the observed hippocampal clusters in the voxel-wise analysis lend credence of an immunohistochemistry validation.

TSPO-PET is not entirely specific for microglial activation, since activated astrocytes and other cells also express TSPO (Venneti et al., 2013; Vivash and O'Brien, 2016). Furthermore, despite robust performance in rodents, translation of TSPO-PET towards human imaging is hampered by a polymorphism of the TSPO gene that causes different binding affinity among individuals (Cumming et al., 2018; Mizrahi et al., 2012). These current limitations of TSPO-PET leave scope for the development of more specific radiotracers that could distinguish between disease associated and homeostatic microglia (Götzl et al., 2019).

5. Conclusion

Elevated TSPO expression in the amygdala-entorhinal-hippocampal complex in App^{NL-G-F} mice is associated with better spatial learning performance in the Morris water maze. This association was stronger for mice with right predominance of elevated TSPO expression in the amygdala. These findings indicate that asymmetric microglial activation is important to maintain brain function in the face of genetically-driven amyloid accumulation.

Data_statement

Imaging data are available in nifti format and can be transferred per request by the corresponding author. Behavioral, biochemical and immunohistochemical data are available in table format on Mendeley Data.

Disclosure

P.B., A.R. and M.B. received speaking honoraria from Life Molecular Imaging and GE healthcare. M.B. is an advisor of Life Molecular Imaging. No other potential conflicts of interest relevant to this article exist.

Credit authorship contribution statement

Gloria Biechele: Formal analysis, Writing - original draft, Investigation, Validation, Methodology. **Karin Wind:** Formal analysis, Investigation, Writing - review & editing. **Tanja Blume:** Formal analysis, Investigation, Writing - review & editing, Methodology. **Christian Sacher:** Formal analysis, Investigation, Writing - review & editing. **Leonie Beyer:** Investigation, Writing - review & editing, Funding acquisition. **Florian Eckenweber:** Investigation, Writing - review & editing. **Nicolai Franzmeier:** Investigation, Writing - review & editing. **Michael Ewers:** Investigation, Writing - review & editing. **Benedikt Zott:** Investigation, Resources, Writing - review & editing. **Simon Lindner:** Investigation, Resources, Writing - review & editing. **Franz-Josef Gildehaus:** Investigation, Resources, Writing - review & editing. **Barbara von Ungern-Sternberg:** Investigation, Writing - review & editing. **Sabina Tahirovic:** Conceptualization, Resources, Writing - review & editing. **Michael Willem:** Conceptualization, Resources, Writing - review & editing. **Peter Bartenstein:** Conceptualization, Resources, Writing - review & editing. **Paul Cumming:** Writing - review & editing, Supervision. **Axel Rominger:** Conceptualization, Supervision, Writing - review & editing. **Jochen Herms:** Conceptualization, Supervision, Writing - review & editing, Project administration. **Matthias Brendel:** Conceptualization, Formal analysis, Supervision, Writing - original draft, Funding acquisition, Writing - review & editing, Project administration.

Supplementary materials

Supplementary material associated with this article can be found, in the online version, at doi:10.1016/j.neuroimage.2020.117707.

References

Bannerman, D.M., Yee, B.K., Lemaire, M., Wilbrecht, L., Jarrard, L., Iversen, S.D., Rawlins, J.N., Good, M.A., 2001. The role of the entorhinal cortex in two forms of spatial learning and memory. Exp. Brain Res. 141, 281–303.

Benjamini, Y., Hochberg, Y., 1995. Controlling the false discovery rate: a practical and powerful approach to multiple testing. J. Royal Stat. Soc.: Ser. B (Methodol.) 57, 289–300.

Bromley-Brits, K., Deng, Y., Song, W., 2011. Morris water maze test for learning and memory deficits in Alzheimer's disease model mice. J. Vis. Exp.

Bryan, K.J., Lee, H., Perry, G., Smith, M.A., Casadesus, G., 2009. Transgenic mouse models of Alzheimer's Disease: behavioral testing and considerations. In: nd, Buccafusco, J.J. (Ed.), Methods of Behavior Analysis in Neuroscience. Boca Raton (FL), Frontiers in Neuroscience.

Catafau, A.M., Bullich, S., Seibyl, J.P., Barthel, H., Ghetti, B., Leverenz, J., Ironside, J.W., Schulz-Schaeffer, W.J., Hoffmann, A., Sabri, O., 2016. Cerebellar Amyloid-beta Plaques: how frequent are they, and do they influence 18F-Florbetaben SUV ratios? J. Nucl. Med. 57, 1740–1745.

Chen, X., Chen, C., Fan, S., Wu, S., Yang, F., Fang, Z., Fu, H., Li, Y., 2018. Omega-3 polyunsaturated fatty acid attenuates the inflammatory response by modulating microglia polarization through SIRT1-mediated deacetylation of the HMGB1/NF-kappaB pathway following experimental traumatic brain injury. J. Neuroinflamm. 15, 116.

Chumbley, J.R., Friston, K.J., 2009. False discovery rate revisited: FDR and topological inference using Gaussian random fields. Neuroimage 44, 62–70.

Cumming, P., Burgher, B., Patkar, O., Breakspear, M., Vasdev, N., Thomas, P., Liu, G.J., Banati, R., 2018. Sifting through the surfeit of neuroinflammation tracers. J. Cereb. Blood Flow Metab. 38, 204–224.

Ehret, G., 1987. Left hemisphere advantage in the mouse brain for recognizing ultrasonic communication calls. Nature 325, 249–251.

El-Gaby, M., Shipton, O.A., Paulsen, O., 2015. Synaptic plasticity and memory: new insights from Hippocampal left-right asymmetries. Neuroscientist 21, 490–502.

Ewers, M., Biechele, G., Suarez-Calvet, M., Sacher, C., Blume, T., Morenas-Rodriguez, E., Deming, Y., Piccio, L., Cruchaga, C., Kleinberger, G., Shaw, L., Trojanowski, J.Q., Herms, J., Dichgans, M., Brendel, M., Haass, C., Franzmeier, N.Alzheimer's Disease Neuroimaging, I., 2020. Higher CSF sTREM2 and microglia activation are associated with slower rates of beta-amyloid accumulation. EMBO Mol. Med. 12 (9), e12308.

Focke, C., Blume, T., Zott, B., Shi, Y., Deussing, M., Peters, F., Schmidt, C., Kleinberger, G., Lindner, S., Gildehaus, F.J., Beyer, L., von Ungern-Sternberg, B., Bartenstein, P., Ozmen, L., Baumann, K., Dorostkar, M.M., Haass, C., Adelsberger, H., Herms, J., Rominger, A., Brendel, M., 2019. Early and longitudinal microglial activation but not amyloid accumulation predicts cognitive outcome in PS2APP mice. J. Nucl. Med. 60, 548–554.

Frings, L., Hellwig, S., Spehl, T.S., Bormann, T., Buchert, R., Vach, W., Minkova, L., Heimbach, B., Kloppel, S., Meyer, P.T., 2015. Asymmetries of amyloid-beta burden and neuronal dysfunction are positively correlated in Alzheimer's disease. Brain 138, 3089–3099.

Frost, G.R., Longo, V., Li, T., Jonas, L.A., Judenhofer, M., Cherry, S., Koutcher, J., Lekaye, C., Zanzonico, P., Li, Y.M., 2020. Hybrid PET/MRI enables high-spatial resolution, quantitative imaging of amyloid plaques in an Alzheimer's disease mouse model. Sci. Rep. 10, 10379.

Goto, K., Kurashima, R., Gokan, H., Inoue, N., Ito, I., Watanabe, S., 2010. Left-right asymmetry defect in the hippocampal circuitry impairs spatial learning and working memory in IV mice. PLoS One 5, e15468.

Götzl, J.K., Brendel, M., Werner, G., Parhizkar, S., Sebastian Monasor, L., Kleinberger, G., Colombo, A.V., Deussing, M., Wagner, M., Winkelmann, J., Diehl-Schmid, J., Levin, J., Fellerer, K., Reifschneider, A., Bultmann, S., Bartenstein, P., Rominger, A., Tahirovic, S., Smith, S.T., Madore, C., Butovsky, O., Capell, A., Haass, C., 2019. Opposite microglial activation stages upon loss of PGRN or TREM2 result in reduced cerebral glucose metabolism. EMBO Mol. Med. e9711.

Heneka, M.T., Carson, M.J., El Khoury, J., Landreth, G.E., Brosseron, F., Feinstein, D.L., Jacobs, A.H., Wyss-Coray, T., Vitorica, J., Ransohoff, R.M., Herrup, K., Frautschy, S.A., Finsen, B., Brown, G.C., Verkhratsky, A., Yamanaka, K., Koistinaho, J., Latz, E., Halle, A., Petzold, G.C., Town, T., Morgan, D., Shinohara, M.L., Perry, V.H., Holmes, C., Bazan, N.G., Brooks, D.J., Hunot, S., Joseph, B., Deigendesch, N., Garaschuk, O., Boddeke, E., Dinarello, C.A., Breitner, J.C., Cole, G.M., Golenbock, D.T., Kummer, M.P., 2015. Neuroinflammation in Alzheimer's disease. Lancet Neurol. 14, 388–405.

Huber, C.M., Yee, C., May, T., Dhanala, A., Mitchell, C.S., 2018. Cognitive decline in preclinical Alzheimer's disease: Amyloid-Beta versus Tauopathy. J. Alzheimers Dis. 61, 265–281.

Jagust, W.J., Landau, S.M., Shaw, L.M., Trojanowski, J.Q., Koeppe, R.A., Reiman, E.M., Foster, N.L., Petersen, R.C., Weiner, M.W., Price, J.C., Mathis, C.A.Alzheimer's Disease Neuroimaging, I., 2009. Relationships between biomarkers in aging and dementia. Neurology 73, 1193–1199.

Maren, S., 1999. Long-term potentiation in the amygdala: a mechanism for emotional learning and memory. Trends Neurosci. 22, 561–567.

Masuda, A., Kobayashi, Y., Kogo, N., Saito, T., Saido, T.C., Itohara, S., 2016. Cognitive deficits in single App knock-in mouse models. Neurobiol. Learn. Mem. 135, 73–82.

Miyashita, Y., 2004. Cognitive memory: cellular and network machineries and their top–down control. Science 306, 435–440.

Mizrahi, R., Rusjan, P.M., Kennedy, J., Pollock, B., Mulsant, B., Suridjan, I., De Luca, V., Wilson, A.A., Houle, S., 2012. Translocator protein (18 kDa) polymorphism (rs6971) explains in-vivo brain binding affinity of the PET radioligand [(18)F]-FEPPA. J. Cereb. Blood Flow Metab. 32, 968–972.

Ossenkoppele, R., Schonhaut, D.R., Scholl, M., Lockhart, S.N., Ayakta, N., Baker, S.L., O'Neil, J.P., Janabi, M., Lazaris, A., Cantwell, A., Vogel, J., Santos, M., Miller, Z.A., Bettcher, B.M., Vossel, K.A., Kramer, J.H., Gorno-Tempini, M.L., Miller, B.L., Jagust, W.J., Rabinovici, G.D., 2016. Tau PET patterns mirror clinical and neuroanatomical variability in Alzheimer's disease. Brain 139, 1551–1567.

Overhoff, F., Brendel, M., Jaworska, A., Korzhova, V., Delker, A., Probst, F., Focke, C., Gildehaus, F.J., Carlsen, J., Baumann, K., Haass, C., Bartenstein, P., Herms, J., Rominger, A., 2016. Automated spatial brain normalization and Hindbrain white matter reference tissue give improved [(18)F]-Florbetaben PET Quantitation in Alzheimer's model mice. Front. Neurosci. 10, 45.

Parhizkar, S., Arzberger, T., Brendel, M., Kleinberger, G., Deussing, M., Focke, C., Nuscher, B., Xiong, M., Ghasemigharagoz, A., Katzmarski, N., Krasemann, S., Lichtenthaler, S.F., Muller, S.A., Colombo, A., Monasor, L.S., Tahirovic, S., Herms, J., Willem, M., Pettkus, N., Butovsky, O., Bartenstein, P., Edbauer, D., Rominger, A., Erturk, A., Grathwohl, S.A., Neher, J.J., Holtzman, D.M., Meyer-Luehmann, M., Haass, C., 2019. Loss of TREM2 function increases amyloid seeding but reduces plaque-associated ApoE. Nat. Neurosci. 22, 191–204.

Pedraza, O., Bowers, D., Gilmore, R., 2004. Asymmetry of the hippocampus and amygdala in MRI volumetric measurements of normal adults. J. Int. Neuropsychol. Soc. 10, 664–678.

Rominger, A., Brendel, M., Burgold, S., Keppler, K., Baumann, K., Xiong, G., Mille, E., Gildehaus, F.-J., Carlsen, J., Schlichtiger, J., 2013. Longitudinal assessment of cerebral b-amyloid deposition in mice overexpressing Swedish mutant b-amyloid precursor protein using 18F-florbetaben PET. J. Nucl. Med. 54, 1127–1134.

Roozendaal, B., McReynolds, J.R., McGaugh, J.L., 2004. The basolateral amygdala interacts with the medial prefrontal cortex in regulating glucocorticoid effects on working memory impairment. J. Neurosci. 24, 1385–1392.

Sacher, C., Blume, T., Beyer, L., Biechele, G., Sauerbeck, J., Eckenweber, F., Deussing, M., Focke, C., Parhizkar, S., Lindner, S., Gildehaus, F.J., von Ungern-Sternberg, B., Baumann, K., Tahirovic, S., Kleinberger, G., Willem, M., Haass, C., Bartenstein, P., Cumming, P., Rominger, A., Herms, J., Brendel, M., 2020. Asymmetry of fibrillar plaque burden in amyloid mouse models. J. Nucl. Med. 61 (12), 1825–1831. doi:10.2967/jnumed.120.242750.

Sacher, C., Blume, T., Beyer, L., Peters, F., Eckenweber, F., Sgobio, C., Deussing, M., Albert, N.L., Unterrainer, M., Lindner, S., Gildehaus, F.J., von Ungern-Sternberg, B., Brzak, I., Neumann, U., Saito, T., Saido, T.C., Bartenstein, P., Rominger, A., Herms, J., Brendel, M., 2019. Longitudinal PET monitoring of amyloidosis and microglial activation in a second-generation amyloid-beta mouse model. J. Nucl. Med. 60, 1787–1793.

Saito, T., Matsuba, Y., Mihira, N., Takano, J., Nilsson, P., Itohara, S., Iwata, N., Saido, T.C., 2014. Single App knock-in mouse models of Alzheimer's disease. Nat. Neurosci. 17, 661–663.

Sarter, M., Markowitsch, H.J., 1985. Involvement of the amygdala in learning and memory: a critical review, with emphasis on anatomical relations. Behav. Neurosci. 99, 342–380.

Shinohara, Y., Hirase, H., Watanabe, M., Itakura, M., Takahashi, M., Shigemoto, R., 2008. Left-right asymmetry of the hippocampal synapses with differential subunit allocation of glutamate receptors. Proc. Natl. Acad. Sci. U. S. A. 105, 19498–19503.

Shinohara, Y., Hosoya, A., Yamasaki, N., Ahmed, H., Hattori, S., Eguchi, M., Yamaguchi, S., Miyakawa, T., Hirase, H., Shigemoto, R., 2012. Right-hemispheric dominance of spatial memory in split-brain mice. Hippocampus 22, 117–121.

Shipton, O.A., El-Gaby, M., Apergis-Schoute, J., Deisseroth, K., Bannerman, D.M., Paulsen, O., Kohl, M.M., 2014. Left-right dissociation of hippocampal memory processes in mice. Proc. Natl. Acad. Sci. U. S. A. 111, 15238–15243.

Suarez-Calvet, M., Kleinberger, G., Araque Caballero, M.A., Brendel, M., Rominger, A., Alcolea, D., Fortea, J., Lleo, A., Blesa, R., Gispert, J.D., Sanchez-Valle, R., Antonell, A., Rami, L., Molinuevo, J.L., Brosseron, F., Traschutz, A., Heneka, M.T., Struyfs, H., Engelborghs, S., Sleegers, K., Van Broeckhoven, C., Zetterberg, H., Nellgard, B., Blennow, K., Crispin, A., Ewers, M., Haass, C., 2016. sTREM2 cerebrospinal fluid levels are a potential biomarker for microglia activity in early-stage Alzheimer's disease and associate with neuronal injury markers. EMBO Mol. Med. 8, 466–476.

Tetzloff, K.A., Graff-Radford, J., Martin, P.R., Tosakulwong, N., Machulda, M.M., Duffy, J.R., Clark, H.M., Senjem, M.L., Schwarz, C.G., Spychalla, A.J., Drubach, D.A., Jack, C.R., Lowe, V.J., Josephs, K.A., Whitwell, J.L., 2018. Regional distribution, asymmetry, and clinical correlates of Tau Uptake on [18F]AV-1451 PET in Atypical Alzheimer's disease. J. Alzheimers Dis. 62, 1713–1724.

Thomason, M.E., Race, E., Burrows, B., Whitfield-Gabrieli, S., Glover, G.H., Gabrieli, J.D., 2009. Development of spatial and verbal working memory capacity in the human brain. J. Cogn. Neurosci. 21, 316–332.

Venneti, S., Lopresti, B.J., Wiley, C.A., 2013. Molecular imaging of microglia/macrophages in the brain. Glia 61, 10–23.

Vivash, L., O'Brien, T.J., 2016. Imaging microglial activation with TSPO PET: lighting up neurologic diseases? J. Nucl. Med. 57, 165–168.

Vorhees, C.V., Williams, M.T., 2006. Morris water maze: procedures for assessing spatial and related forms of learning and memory. Nat. Protoc. 1, 848–858.

Vorhees, C.V., Williams, M.T., 2014. Assessing spatial learning and memory in rodents. ILAR J. 55, 310–332.

Whyte, L.S., Hemsley, K.M., Lau, A.A., Hassiotis, S., Saito, T., Saido, T.C., Hopwood, J.J., Sargeant, T.J., 2018. Reduction in open field activity in the absence of memory deficits in the App(NL-G-F) knock-in mouse model of Alzheimer's disease. Behav. Brain Res. 336, 177–181.

Yue, L., Wang, T., Wang, J., Li, G., Wang, J., Li, X., Li, W., Hu, M., Xiao, S., 2018. Asymmetry of Hippocampus and Amygdala defect in subjective cognitive decline among the community dwelling Chinese. Front. Psychiatry 9, 226.

Zahn, R., Juengling, F., Bubrowski, P., Jost, E., Dykierek, P., Talazko, J., Huell, M., 2004. Hemispheric asymmetries of hypometabolism associated with semantic memory impairment in Alzheimer's disease: a study using positron emission tomography with fluorodeoxyglucose-F18. Psychiatry Res. 132, 159–172.

Ziegler-Graham, K., Brookmeyer, R., Johnson, E., Arrighi, H.M., 2008. Worldwide variation in the doubling time of Alzheimer's disease incidence rates. Alzheimers Dement 4, 316–323.